Online ISSN 1848-3380, Print ISSN 0005-1144
ATKAFF 53(1), 56–68(2012)

Antonio Šarolić, Damir Senić, Zlatko Živković

Radiation Pattern of a Vertical Dipole over Sea and Setup for Measuring thereof

DOI: 10.7305/automatika.53-1.162
UDK 621.396.674.3.08:551.461
IFAC 5.8.3; 3.1

Original scientific paper

In this paper, a compact setup for measuring the radiation pattern of an arbitrary positioned antenna above the sea surface is presented. The antenna of interest was a vertical half-wave dipole. Due to impracticalities concerning the measurements using seaborne platforms, the setup was based around a shallow pool filled with actual sea water. The transmitting antenna-under-test (AUT) and the receiving antenna stands were placed on the solid ground, at the opposite sides of the pool, thus ensuring the stable platforms as well as the wave path over sea. The need for precise positioning of the receiving antenna along the circular path was avoided and the straight measurement line was used instead, yielding further simplification of the method. Both antennas were realized as printed half-wave dipoles. The measurements were carried out in ISM frequency band at 2.48 GHz. The chosen frequency enabled the realization of a compact setup for elevation radiation pattern measurements for AUT heights up to 2λ above the sea surface. The measurement results were compared to the theoretical and simulation results for a half-wave dipole over sea, showing a good agreement. Detailed evaluation of the measurement uncertainty was undertaken, indicating the critical points in the realized setup.

Key words: Antenna above sea surface, Lossy dielectric ground plane, Radiation pattern measurement setup, Vertical half-wave dipole

Dijagram zračenja vertikalnog dipola iznad mora i mjerni postav za njegovo mjerenje. U ovom radu predstavljen je kompaktni postav za mjerenje dijagrama zračenja proizvoljno postavljene antene iznad površine mora. Predmet analize je vertikalni poluvalni dipol. S obzirom na nepraktičnost mjerenja na plovećoj platformi, postav se temelji na plitkom bazenu napunjenom stvarnom morskom vodom. Stativi za ispitivanu odašiljačku antenu i prijamnu antenu postavljeni su na čvrstom tlu na nasuprotnim stranama bazena, tako da se antene nalaze na stabilnim platformama, a putanja vala se nalazi u potpunosti iznad mora. Dodatna značajka predložene metode jest pravocrtno pomicanje prijamne antene tijekom mjerenja dijagrama zračenja. Time je izbjegnuta potreba preciznog pozicioniranja po kružnoj putanji, što je dovelo do dodatnog pojednostavnjenja metode. Obje antene izrađene su kao poluvalni dipoli u planarnoj tehnologiji. Mjerenja su provedena na ISM frekvenciji od 2.48 GHz. Odabrana frekvencija omogućuje izradu kompaktnog postava za mjerenje vertikalnog dijagrama zračenja za visine odašiljačke antene do 2λ iznad morske površine. Mjerni rezultati pokazuju dobro slaganje s analitičkim rezultatima i rezultatima simulacije za poluvalni dipol iznad mora. Provedena je i prikazana detaljna procjena mjerne nesigurnosti, kao pokazatelj kritičnih točaka u realiziranom postavu.

Ključne riječi: antena iznad mora, dielektrik s gubicima, uzemljena ravnina, mjerni postav za mjerenje dijagrama zračenja, vertikalni poluvalni dipol

1 INTRODUCTION

The dipole antenna above a ground plane is a well-known theoretical problem [1-4] that presents the important background for many practical issues, especially in maritime and mobile applications [5-7].

Depending on the application, the antenna height above the ground plane usually varies up to several wavelengths, causing the well-known lobing effect shown in [1] and [3-4]. Although the theoretical radiation characteristics of a vertical dipole are common subject in the literature, there is evident lack of measurements performed in the real environment, especially at sea. Analyses of such radiating structures are mainly based on the numerical methods implemented by simulation software as a powerful tool for solving the shipboard electromagnetic problems [8-9]. However, actual measurements are of utmost importance, giving us the valuable insights into the physical phenomena and making possible the verification of the simulation

and/or theoretical results [10-14].

To the best of our knowledge, in available literature, there are only a few references dealing with measurement of radiation pattern of an antenna above the sea surface. The measurement setups described in literature were intended for specific problems and relied on considerable resources: in [11] the horizontal (azimuthal) radiation pattern was measured along the 4.6 NM long path from the ship to the shore, in [12] the vertical (elevation) pattern was measured using 70-foot high wooden arch above the antenna over sea, in [13] airborne measurements were done using a dirigible.

The aim of this study was to produce a compact, reliable and affordable measurement setup capable for measuring the radiation pattern of an antenna above the sea surface. The setup was engineered, realized and used for several sets of measurements, using a vertical half-wave dipole as the antenna under test (AUT). The overview of some preliminary results and measurement procedures has been presented in [14]. This paper gives the detailed description of the proposed method and the realized setup, along with the results for a set of consistent measurements comparable to analytical results.

In section 2, the analytical solution for radiation pattern of the vertical half-wave dipole above the sea surface, together with the analytical and simulation results, is given. The detailed explanation of the measurement method and setup is presented in the section 3. The measurement results for the radiation pattern of a vertical half-wave dipole over sea are presented in section 4, compared to the analytical results and shown together with the boundaries of measurement uncertainty. The measurement uncertainty is calculated in section 5, where the detailed uncertainty budget is presented. The final remarks are given in the conclusion at the end.

2 RADIATION PATTERN OF A VERTICAL DIPOLE ABOVE A LOSSY DIELECTRIC GROUND PLANE

A vertical half-wave dipole antenna is placed in the air, along *z*-axis, at a certain height *h* above a lossy dielectric ground plane having characteristics of sea water (Fig. 1). The analysis of the radiation pattern of a vertical dipole antenna with the sinusoidal current distribution above a ground plane can start from the well-known expression for the radiation pattern of an infinitesimal vertical electric dipole above a ground plane [1]:

$$F_\vartheta^i = \sin\vartheta \cdot \left| e^{j\beta_0 h\cos\vartheta} + R_v e^{-j\beta_0 h\cos\vartheta} \right|, \qquad (1)$$

where ϑ is the elevation angle in spherical coordinate system, $\beta_0 = 2\pi/\lambda$ is the phase constant for free space, λ is the wavelength in free space and *h* is the height of the antenna above the ground plane.

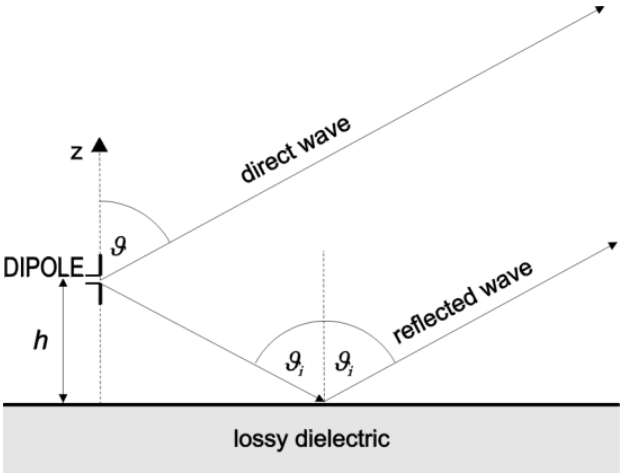

Fig. 1. Vertical dipole above the lossy dielectric.

The expression (1) is based on the pattern multiplication rule, where $\sin\vartheta$ is the radiation pattern of the infinitesimal vertical dipole, and the rest of the expression represents the array factor of a two-element array formed by the dipole and its image below the ground plane. If a half-wave dipole is used instead, its radiation pattern is used instead of $\sin\vartheta$:

$$F_\vartheta = \frac{\cos\left(\frac{\pi}{2}\cos\vartheta\right)}{\sin\vartheta} \cdot \left| e^{j\beta_0 h\cos\vartheta} + R_v e^{-j\beta_0 h\cos\vartheta} \right|. \qquad (2)$$

These expressions are valid in the far field, where the approximation of parallel direct and reflected waves can be used (Fig. 1). For such approximation, Fresnel reflection coefficient R_v for oblique incidence of a parallelly polarized EM wave upon a planar interface between the air and a lossy medium is defined by [1] and [15]:

$$R_v = \frac{\eta_0\cos\vartheta_i - \eta\cos\psi}{\eta_0\cos\vartheta_i + \eta\cos\psi}, \qquad (3)$$

where ϑ_i is the angle of incidence (for the approximation of parallel direct and reflected waves, $\vartheta_i = \vartheta$, as seen in Fig. 1), ψ is the angle of refraction, η_0 and η are the wave impedances of the air and the non-magnetic lossy dielectric, respectively:

$$\eta_0 = \sqrt{\frac{\mu_0}{\varepsilon_0}}, \qquad \eta = \sqrt{\frac{j\omega\mu_0}{\sigma + j\omega\varepsilon}}, \qquad (4)$$

where μ_0 and ε_0 are permeability and permittivity of free space, σ is the conductivity and ε is the permittivity of the lossy dielectric, where $\varepsilon = \varepsilon_0\varepsilon_\mathrm{r}$, ($\varepsilon_\mathrm{r}$ is the relative permittivity of the lossy dielectric), and ω is the angular frequency.

According to [15], the angle ψ can be obtained as:

$$\psi = \operatorname{arctg}\frac{t}{q}, \tag{5}$$

where

$$t = \beta_0 \sin\vartheta_i = \omega\sqrt{\mu_0\varepsilon_0}\sin\vartheta_i, \tag{6}$$

$$q = Re\{\gamma_0\} \cdot Im\{s\} + Im\{\gamma_0\} \cdot Re\{s\}, \tag{7}$$

while s is the complex number obtained by:

$$s = \sqrt{1 - \left(\frac{\gamma_0}{\gamma} \cdot \sin\vartheta_i\right)^2}, \tag{8}$$

and γ_0 and γ are the propagation constants in the air and in the lossy medium, respectively:

$$\gamma_0 = j\omega\sqrt{\mu_0\varepsilon_0}, \quad \gamma = \sqrt{j\omega\mu_0(\sigma + j\omega\varepsilon)}. \tag{9}$$

The electric parameters of sea water at 2.48 GHz for 20°C are taken from [16] as σ = 6.5 S/m and $\varepsilon_r = 70$. The radiation pattern calculated using (2) – (9) is given in Fig. 2, for several antenna heights of interest, as the function of incident angle ϑ_i. Polar plot of the elevation radiation pattern of a vertical half-wave dipole at $h = 2\lambda$ was calculated using Numerical Electromagnetics Code (NEC) [17] and presented in Fig. 3.

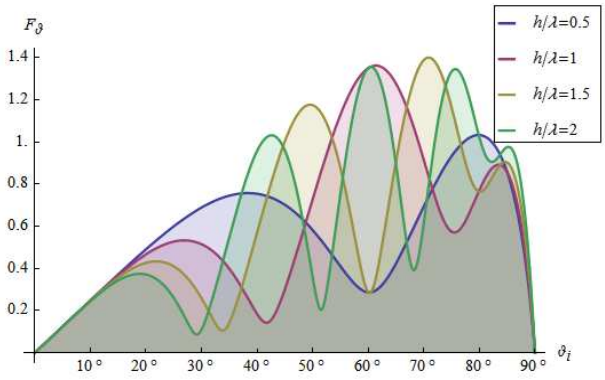

Fig. 2. Elevation patterns calculated using (2).

3 MEASUREMENT SETUP AND METHOD

3.1 Aim and Scope

The goal of the study was to measure the vertical (elevation) radiation pattern of the vertical half-wave dipole TX antenna above the sea surface. Since the initial motivation for the study was to analyze maritime communications that use vertically polarized antennas and waves, the measurement was done specifically for the vertically polarized component, i.e. using vertical half-wave dipole RX antenna.

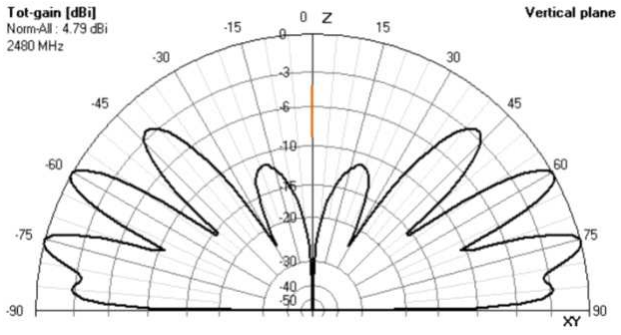

Fig. 3. Elevation pattern for h = 2λ (NEC simulation using [17]).

Due to the limitations explained in section 3.4, and the procedure explained in section 3.5, the setup is most suitable for measuring the lower part of the elevation pattern. Considering the stated motivation, we chose to measure the pattern starting from the horizon and up to 45° above the horizon, where the maritime (terrestrial) communication actually occurs. Hence, the angles higher than 45° above the horizon were not measured.

3.2 Principles of the Measurement Setup

When considering the need for measuring the antenna radiation pattern over sea, seaborne platforms are the first idea. However, using seaborne platforms would present several serious problems to solve. The elevation pattern of the AUT (antenna under test) should be measured by continuously varying the height of the measuring antenna. This is not easily achievable onboard a ship. Furthermore, the floating platforms do not stand still. Therefore, the inability to fine-control the TX and RX antenna positions and polarizations would reflect in the measurement geometry problems. To decrease the angle error arising from the antenna position fluctuation, the TX and RX antennas would have to be largely separated to a far distance. This would render the pattern measurement almost impossible for higher angles above the horizon, because the proper measuring antenna heights would be even more difficult to achieve. Last but not least, the flatness (or the roughness) of the sea surface should be controlled in order to properly interpret the results. This is hardly achievable at sea because there is always some kind of swell present. Even with no wind, there are surface fluctuations due to distant swells or, more often and unavoidable, due to ships passing by (Fig. 4).

To avoid almost all these problems, we realized the propagation path over the sea surface using a pool filled with sea water (Fig. 4). The precision of the TX and RX antenna positions and polarizations was secured by placing their stands on the solid ground on the opposite sides

Fig. 4. Measurement setup. No wind blowing: pool surface perfectly flat, sea surface not.

of the pool. The AUT was set up as the TX antenna, while the RX antenna was used for measurement. The flatness of the surface was perfect in the calm conditions without wind.

The pool depth had to be determined to match the conditions at the deep sea, i.e. to be able to disregard any effect of the wave transmitted beneath the sea surface. In the real conditions, the transmitted wave gets attenuated fast by the lossy medium. The reflection from the sea bed is therefore irrelevant and the transmitted wave will not arise above the surface again. This eliminates any interference of the transmitted wave with the incident and reflected wave above the surface. The pool depth should be properly determined to ensure enough attenuation.

The last issue was to determine the size of the setup, with respect to mandatory far-field conditions, considering the size of the antenna system (formed by the AUT and its image below the ground plane). The far-field requirement determined the pool length, while the maximum measured elevation in the pattern was determined by the achievable height of the measuring antenna. The former (pool length) was not as limiting factor as was the latter (measuring the antenna height). The optimum frequency had to be chosen to satisfy all requirements. The pool width was not considered critical and its dimension was chosen to ensure a wide-enough propagation path over sea, however keeping the setup as compact as possible.

Another practical requirement for the setup was to place it near the sea, as to be able to fill the pool with the large volume of sea water using a water pump. To be able to properly control the geometry and to minimize the pool volume, the pool had to be placed on a firm flat surface. The transmission was directed away from the land towards the open sea. This could be useful for a directional AUT, to avoid reflections from eventual obstacles on land, but is not as important for an omnidirectional AUT. The electromagnetic requirement was to avoid any scattering objects in the vicinity of the setup. Also, the conductive material should be completely avoided in the setup construction. The setup should be easily dismountable and moveable to a chosen location.

3.3 Pool Depth

The pool should be deep enough to avoid the possibility that the transmitted wave gets reflected by the pool bottom, and appears again above the pool surface. To ensure deep sea conditions, the attenuation of the electromagnetic wave passing twice through the 10 cm thick layer of sea water was calculated. The calculation was performed assuming the worst-case scenario that includes normal incidence and total reflection from the pool bottom. Regarding the plane-wave propagation through a given medium, the attenuation coefficient α is given by [15]:

$$\alpha = \omega\sqrt{\mu_0\varepsilon}\sqrt{\frac{1}{2}\left[\sqrt{1+\left(\frac{\sigma}{\omega\varepsilon}\right)^2}-1\right]}, \qquad (10)$$

where quantities are defined as in (4). Attenuation in dB can be calculated by:

$$ATT = 20\log\left(e^{2\cdot d_{\mathrm{p}}\cdot\alpha}\right), \qquad (11)$$

where d_{p} is the pool depth. For the specified pool depth of 0.1 m and the electric parameters of the sea water [16] at 2.48 GHz ($\sigma = 6.5$ S/m and $\varepsilon_{\mathrm{r}} = 70$), the attenuation was calculated to be in the range of $>$200 dB, which is more than sufficient to simulate the deep sea and to neglect any effect of the transmitted wave.

3.4 Realization of the Measurement Setup

The overall setup dimensions were determined considering the minimum necessary distance between the TX and the RX antenna that would ensure the far-field conditions. For known wavelength λ and the greatest overall dimension of the antenna system *D*, the far-field boundary R_{FF} can be calculated:

$$R_{\mathrm{FF}} = \frac{2D^2}{\lambda}. \qquad (12)$$

The antenna system (i.e. antenna array) is formed by the original antenna and its image beneath the sea surface (ground plane). Hence, the overall dimension *D* of the antenna system equals:

$$D = 2\cdot h + 2\cdot\frac{\lambda}{4} = 2\cdot h + \frac{\lambda}{2}, \qquad (13)$$

where *h* is the AUT height above the sea surface, while $2{\cdot}\lambda/4$ represents the lengths of the dipole arms that extend beyond 2*h*.

The practical limit in achieving the controllable RX antenna height was, in our case, around 4 m. Considering that the goal was to measure the pattern up to the elevation of 45° above the horizon, we decided to build a setup based on the 4 m × 1 m pool (Fig. 5).

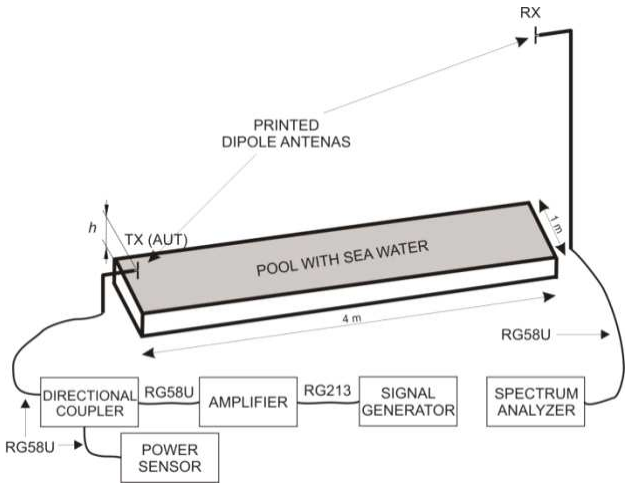

Fig. 5. Schematic layout of measurement setup.

The pool length defines the length of the shortest direct wave path, thus it should be longer than the far-field boundary R_{FF}. Considering the wavelength and (12) – (13), these pool dimensions are appropriate for measurements in 2.4 GHz ISM frequency band, for AUT heights up to 1.8λ. We chose to measure at the frequency of 2.48 GHz, and for the AUT heights of 0.5λ, 1λ, 1.25λ, and 1.5λ. As the far-field boundary calculated by (12) is not a sharp measure, we chose to measure also for the AUT height of 2λ.

At the defined frequency, the printed half-wave dipole (Fig. 6) was easily realized as in [18], and used as the transmitting and the receiving antenna.

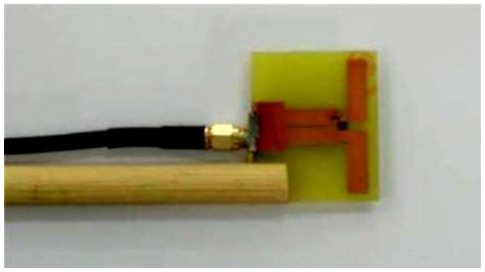

Fig. 6. Printed half-wave dipole used for TX and RX.

The RX antenna was placed on a wooden tripod with adjustable height. The AUT holder was made of wood and plastic, as well as all other parts of the pool and antenna supports.

Due to thickness of the pool walls (wooden boards) and the construction details, the achieved length of the propagation path, i.e. the distance between the system origin and the RX antenna, was 3.95 m.

The signal was generated by the RF signal generator Rohde&Schwarz SM300 working in CW mode at 2.48 GHz, and amplified by 10 W RF amplifier Ophir 5140. The TX power was monitored with Rohde&Schwarz NRP-Z21 power sensor and kept constant. It is worth noting that the power was quite stable throughout the measurements and adjustments were not even needed. The RX power was measured by the spectrum analyzer Anritsu MS2663C.

3.5 Measurement Procedure

The intuitive approach to radiation pattern measurement would be to measure the field along the circular path around the AUT (shown in Fig. 7), ensuring constant radius between the TX and RX antenna. However, this would pose significant difficulties in terms of precise positioning of the RX antenna. The RX antenna, mounted on the tripod, would have to pass along this curved path, measuring the received power at the discrete elevation angles (according to chosen angular resolution). This would imply the simultaneous adjustment of two dimensions (horizontal and vertical distance from the coordinate system origin, d_{H} and d_{V}, respectively, see Fig. 7). This procedure was tested first, and it proved to be problematic and time consuming. Instead, we chose to measure along the vertical measurement line, as shown in Fig. 7. In this way, only one dimension, d_{V}, had to be adjusted, while d_{H} was kept constant at 3.95 m, which was far easier to achieve.

The height of the receiving antenna d_{V} had to be adjusted to the pre-calculated discrete values, according to the chosen angular resolution and:

$$d_{\mathrm{V}} = d_{\mathrm{H}} \cdot \mathrm{tg}\delta = 3.95\mathrm{m} \cdot \mathrm{tg}\delta, \tag{14}$$

where δ is the elevation angle above the horizon. However, this meant that the measured RX power had to be corrected because it was not measured at a constant radius *r*, but at the distance increased by Δr. Since the RX power is proportional to $1/r^2$, the RX power used for radiation pattern measurement had to be corrected, i.e. increased by the factor of $(r+\Delta r)^2/r^2$:

$$P_r = P_{r+\Delta r} \cdot \left(\frac{r+\Delta r}{r}\right)^2, \tag{15}$$

where P_r is the received power at the constant radius of 3.95 m (used for radiation pattern calculation), $P_r + \Delta r$

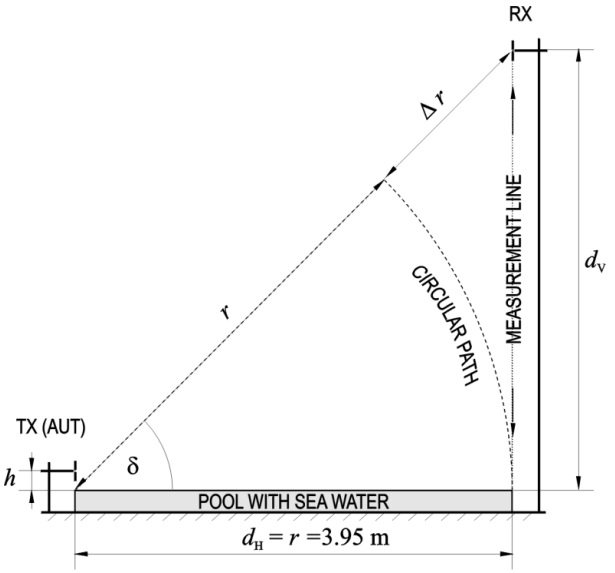

Fig. 7. Geometry of the measurement setup.

is the measured received power, and Δr can be precalculated for angles of interest from the geometry shown in Fig. 7:

$$\cos\delta = \frac{r}{r+\Delta r} \Rightarrow \Delta r = \frac{r\,(1-\cos\delta)}{\cos\delta}. \qquad (16)$$

In order to obtain the elevation radiation pattern in acceptable resolution, the angle range of 45° was divided in 15 steps of 3°, yielding 16 measurements for every single measurement procedure. The RX antenna height d_V was measured using 5 m long telescopic rod equipped with a level for control of the rod verticality.

4 MEASUREMENT RESULTS

The measurement results for the AUT heights of 0.5λ, 1λ, 1.25λ, 1.5λ and 2λ are given in Fig. 8 to Fig. 12. The results are presented together with the boundaries of the measurement uncertainty (expanded uncertainty, coverage factor k = 2), which was evaluated in detail in section 5, for each AUT height.

The theoretical results were obtained for an ideal half-wave dipole over sea, using analytical relations (2) – (9), and are also shown in figures. As explained in section 3.1, all results refer to the vertical component of the electric field, thus the analytical results were obtained by multiplying (2) with $\sin\vartheta$.

All results were measured and presented as relative values. We were not interested in the absolute values of the incident field or RX power.

To be able to compare the measured and the theoretical radiation pattern, they should be overlapped as logically

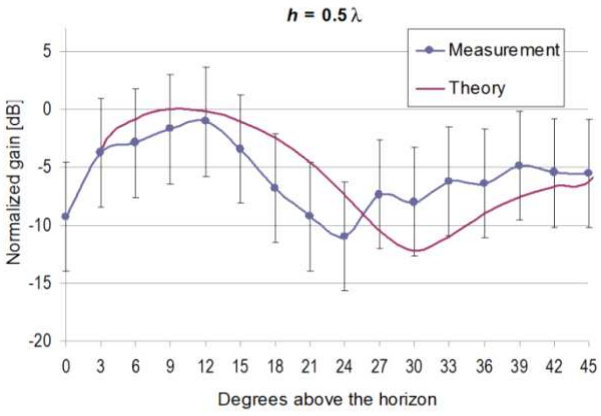

Fig. 8. Radiation pattern for h = 0.5λ, expanded uncertainty (k = 2): ±4.683 dB.

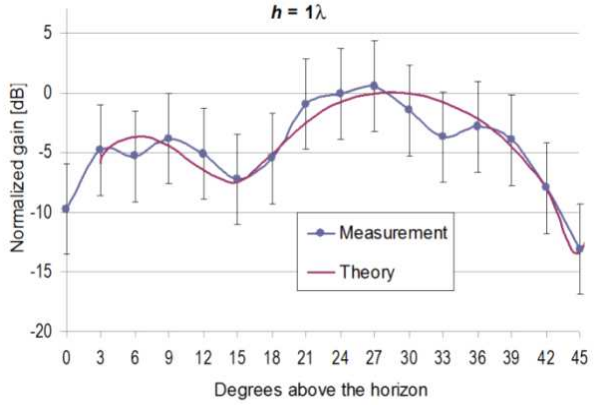

Fig. 9. Radiation pattern for h = 1λ, expanded uncertainty (k = 2): ±3.776 dB.

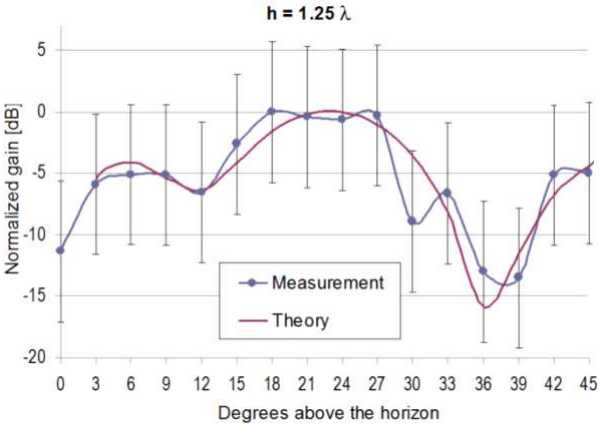

Fig. 10. Radiation pattern for h = 1.25λ, expanded uncertainty (k = 2): ±5.721 dB.

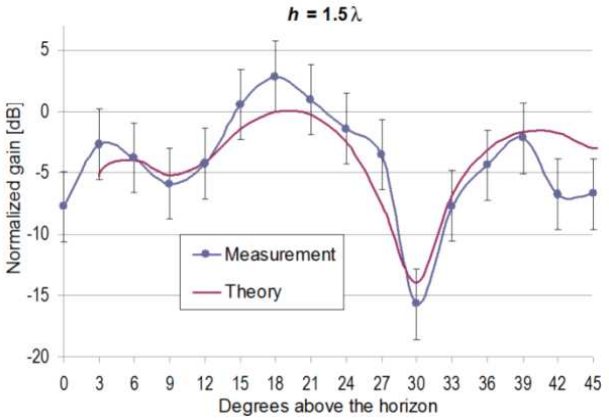

Fig. 11. Radiation pattern for h = 1.5λ, expanded uncertainty (k = 2): ±2.850 dB.

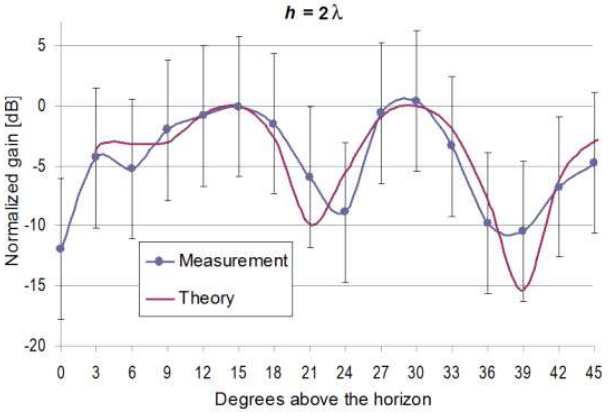

Fig. 12. Radiation pattern for h = 2λ, expanded uncertainty (k = 2): ±5.840 dB.

as possible. Since there was no absolute reference for the graphs, first the theoretical radiation pattern was normalized to the maximum value, i.e. the maximum value of the theoretical radiation pattern became the 0 dB reference. Then the measured results in dB were compared to the previously calculated normalized theoretical values for each angle, and the mean signed absolute error was calculated as

$$\frac{1}{N}\sum_{i=1}^{N}\left(x_{i\mathrm{dB}}^{measured}-x_{i\mathrm{dB}}^{theory}\right), \tag{17}$$

where x_i is the result in dB at i^{th} point, and *N* is the number of points. This mean error value in dB was applied as the offset value to each measurement result. This resulted with a new set of values that corresponded to the measurement results and still kept their relative ratios. However, the mean signed absolute error between the theoretical and the measurement results was thus eliminated, ensuring the most logical overlapping of two graphs in each figure.

The first point ($\delta = 0$) was excluded from this operation (thus *N* = 15 in (17)), since the error was too big. This happened because the theoretical result for $\delta = 0$ should be zero, or, in dB: $-\infty$. However, we could not make the measurement at exactly $\delta = 0$, due to finite dimensions of the RX antenna (the RX antenna is not infinitesimally small). The measured result at δ = 0 thus does not refer exactly to $\delta = 0$, but to the lowest point (lowest angle above the horizon) that could be achieved with the RX antenna, when the tip of the lower dipole arm was almost touching the sea water. For this reason, the theoretical value of $-\infty$ dB is not shown on the graphs.

Graphs show that the theoretical results are in most points contained within the boundaries of measurement expanded uncertainty with coverage factor $k = 2$. Moreover, many points overlap within ±2 dB in all graphs. The accordance is especially good for AUT heights of 1λ and 1.5λ.

It is worth noting that the stated uncertainty refers to the realized setup and not to the proposed method in general. The uncertainty evaluation, given in section 5, shows which particular measurements should be more precise in order to achieve lower uncertainty.

5 EVALUATION OF MEASUREMENT UNCERTAINTY

We proposed a novel method, realized the prototype setup, and made the preliminary measurements. In order to analyze the critical points in the realized setup, we have also established the measurement uncertainty budget. This should prove useful for subsequent setup realizations and measurements.

The evaluation was done using principles given in [19] and [20] for Type B evaluation of standard uncertainty.

5.1 Functional relationships

Individual contributions to the combined uncertainty can be properly assessed using the mathematical function that expresses the dependence of the result on the measured quantities. Radiation pattern measurement is based on measurement of the received power that can be expressed using the expression based on Friis equation, modified according to our setup. The received power is given by equation (all quantities in dB):

$$\begin{aligned}P_{\mathrm{RXdB}} = {} & P_{\mathrm{TX}} + G_{\mathrm{TX}} + G_{\mathrm{RX}} + 10\log\left(\tfrac{\lambda}{4\pi}\right)^2 - \\ & -10\log d^2 + L_{\mathrm{C}} + \mathrm{ME} + 10\log\left(\cos^2\alpha_{\mathrm{TX}}\right) + \\ & +10\log\left(\cos^2\alpha_{\mathrm{RX}}\right) + k_{\Delta r} + 10\log|F|^2\end{aligned} \tag{18}$$

where:

- P_{RX} is the power measured by the spectrum analyzer;
- P_{TX} is the power input to the TX antenna;
- G_{TX} is the gain of the TX antenna, $G_{\mathrm{TX}} = f(\vartheta)$;
- G_{RX} is the gain of the RX antenna, $G_{\mathrm{RX}} = f(\vartheta)$;
- d is the distance from the system origin to RX antenna;
- L_{C} is the overall loss in connecting cables and connectors;
- ME is the mismatch error in the system;
- $\cos^2 \alpha_{\mathrm{TX}}$ is the polarization loss due to the transversal (normal) tilt of the TX antenna, α_{TX} is the tilt angle, $\alpha_{\mathrm{TX}} = 0$ if no tilt;
- $\cos^2 \alpha_{\mathrm{RX}}$ is the polarization loss due to the transversal (normal) tilt of the RX antenna, α_{RX} is the tilt angle, $\alpha_{\mathrm{RX}} = 0$ if no tilt;
- $k_{\Delta r}$ is the correction factor given by (15), calculated for each measurement point (not a measured quantity);
- F is the array factor of the TX antenna system.

However, the radiation pattern is given in relative terms, as the ratio (or difference in dB) between consecutive P_{RX} power measurements for various elevation angles ϑ. Therefore, the uncertainty will be influenced only by quantities that can vary from one measurement to another, i.e. across the whole set of measurements. Only those contributions are taken into account.

5.2 Geometrical relationships

The array factor *F* can be considered as a superposition of the direct and the reflected wave, i.e. the array factor of the two-element antenna array consisting of the AUT and its image below the ground plane:

$$F = 1 + R_v \cdot \mathrm{e}^{-\mathrm{j}\beta\Delta d}, \tag{19}$$

where R_v is the reflection coefficient defined by (3), and Δd is the difference in the distances traveled by the direct and reflected wave (which results in the phase difference between the two waves). Thus, if the direct wave reaches the RX antenna with phase 0°, the phase of the reflected wave shall be $\mathrm{e}^{-\mathrm{j}\beta\Delta d}$. Equation (19) assumes that TX gain is the same for both direct and reflected wave (whole $|F|^2$ is ultimately multiplied by G_{TX}, i.e. added in dB in (18)). This is true if the AUT (vertical dipole) radiation pattern has its maximum pointed towards the horizon, and the main lobe is symmetrical upwards and downwards. However, if the pattern is not symmetrical (e.g. due to slightly unbalanced feed), or if the TX antenna tilts longitudinally, the gain changes by ΔG_{TX}. The change is opposite in sign for the direct and the reflected wave, as seen in Fig. 13. This effect will be the greatest for $\vartheta = 45°$ (the largest change of gain for a tilt angle). This must be included in (19), for later estimation of the uncertainty:

$$|F|^2 = \left|1 + \frac{\Delta G_{\mathrm{TX}}}{G_{\mathrm{TX}}} + \left(1 - \frac{\Delta G_{\mathrm{TX}}}{G_{\mathrm{TX}}}\right) \cdot R_v \cdot \mathrm{e}^{-\mathrm{j}\beta\Delta d}\right|^2. \tag{20}$$

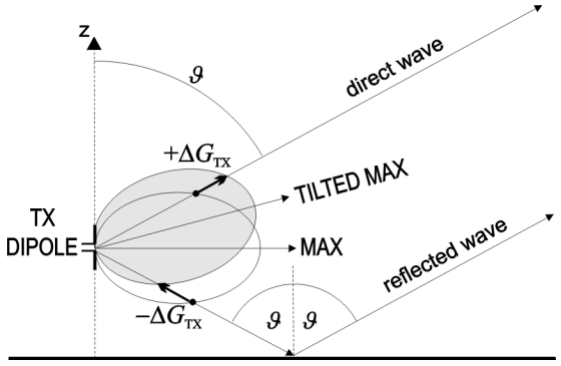

Fig. 13. Effect of longitudinal (parallel) tilt of the TX antenna, for the case of uptilt.

Similar effect of gain change occurs also on the RX side, if the RX antenna is tilted longitudinally or has a non-symmetrical pattern (due to e.g. slightly unbalanced feed). Both the direct and the reflected wave arrive to the RX antenna from the same angle (they are approximately parallel in the far field), thus the gain change is either positive or negative for both waves at the same time (Fig. 14).

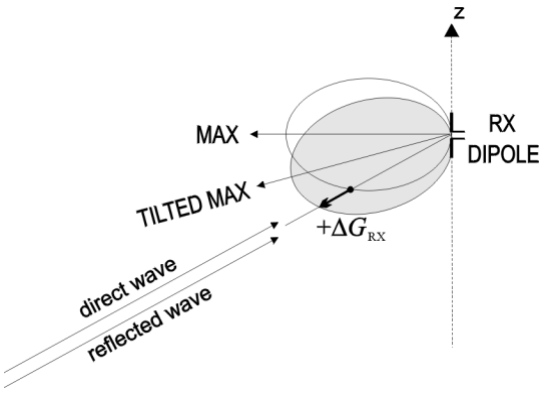

Fig. 14. Effect of longitudinal (parallel) tilt of the RX antenna, for the case of downtilt.

True geometrical relationships can be observed in Fig. 15. The direct wave travels the distance d_{d}, while the re-

flected wave travels a different distance: $d_1 + d_2 = d_\mathrm{r}$. Amplitude-wise, the difference between d_d and d_r can be disregarded and, for both waves, the distance *d* (from the system origin, point O, to the TX antenna) can be used. Its square, used in (18), is a function of two measured quantities d_H and d_V, given by:

$$d^2 = d_\mathrm{H}^2 + d_\mathrm{V}^2. \tag{21}$$

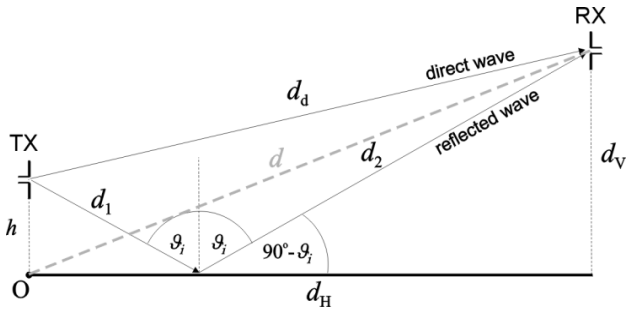

Fig. 15. Geometry basis for phase difference calculation, without the approximation of parallel waves.

However, the difference $\Delta d = d_\mathrm{r} - d_\mathrm{d}$ results in the phase difference between the two waves described by $\mathrm{e}^{-\mathrm{j}\beta\Delta d}$. These quantities can be expressed by the measured quantities *h*, d_H and d_V:

$$d_\mathrm{r} = d_1 + d_2, \tag{22}$$

$$\cos(90^\circ - \vartheta_i) = \frac{d_\mathrm{H}}{d_1 + d_2}, \tag{23}$$

$$\mathrm{tg}(90^\circ - \vartheta_i) = \frac{h + d_\mathrm{V}}{d_\mathrm{H}}, \tag{24}$$

$$d_\mathrm{r} = \frac{d_\mathrm{H}}{\cos(\mathrm{arctg}\frac{h+d_\mathrm{V}}{d_\mathrm{H}})}, \tag{25}$$

$$d_\mathrm{d} = \sqrt{d_\mathrm{H}^2 + (d_\mathrm{V} - h)^2}, \tag{26}$$

$$\Delta d = \frac{d_\mathrm{H}}{\cos(\mathrm{arctg}\frac{h+d_\mathrm{V}}{d_\mathrm{H}})} - \sqrt{d_\mathrm{H}^2 + (d_\mathrm{V} - h)^2}. \tag{27}$$

As R_v and G_TX are functions of ϑ_i, they must be expressed as functions of the measured quantities *h*, d_H and d_V, using (from (24)):

$$\vartheta_i = 90^\circ - \mathrm{arctg}\frac{h + d_\mathrm{V}}{d_\mathrm{H}}. \tag{28}$$

For RX antenna in the far field, $\vartheta = \vartheta_i$, as seen in Fig.1.

5.3 Sensitivity coefficients

If a measurand *Y* is determined from *N* other measured quantities X_1, X_2, ..., X_N through a functional relationship $Y = f(X_1, X_2, \ldots, X_N)$, the combined standard uncertainty $u_\mathrm{c}(y)$ is calculated by [20]:

$$u_\mathrm{c}(y) = \sqrt{\sum_{i=1}^{N} [c_i u(x_i)]^2}, \tag{29}$$

where x_i and *y* are the estimates of the quantities X_i and *Y*, respectively, and c_i is the sensitivity coefficient:

$$c_i = \frac{\partial f}{\partial x_i}, \tag{30}$$

giving the measure of measurand sensitivity to the variation of the quantity X_i. When numerically calculating the value of the obtained partial derivative function, all arguments (quantities) are entered as the values measured (or calculated) in the point of interest. If there are multiple choices, the worst-case scenario with respect to the measurement uncertainty is used.

The sensitivity coefficients for quantities added in dB, as in (18), are obviously equal to 1. This is also true for quantities that are just added together into a final value, such as in distance measurements.

The sensitivity coefficient had to be calculated for the sensitivity of d_2 to quantities d_H and d_V, using (21) and (30), for the worst-case scenario where $d_\mathrm{H} = d_\mathrm{V} = 3.95\,\mathrm{m}$.

As the gains G_TX and G_RX are functions of ϑ (approximately equal to ϑ_i, see Fig. 1 and Fig. 15), due to (28), they are also functions of the measured quantities *h*, d_H and d_V. Functional dependence $G_\mathrm{TX(RX)} = f(h, d_\mathrm{H}, d_\mathrm{V})$ is given by the expression for the gain of half-wave dipole and (28):

$$\begin{aligned} G_\mathrm{TX(RX)} &= \frac{\cos\left(\frac{\pi}{2}\cos\vartheta\right)}{\sin\vartheta} \\ &= \frac{\cos\left[\frac{\pi}{2}\cos\left(90^\circ - \mathrm{arctg}\frac{h+d_\mathrm{V}}{d_\mathrm{H}}\right)\right]}{\sin\left(90^\circ - \mathrm{arctg}\frac{h+d_\mathrm{V}}{d_\mathrm{H}}\right)}. \end{aligned} \tag{31}$$

Therefore, sensitivity coefficients of G_TX and G_RX to all three quantities were found as partial derivatives of (31) with respect to *h*, d_H and d_V, using worst-case values: $h = 0.5\lambda$, $d_\mathrm{H} = d_\mathrm{V} = 3.95\,\mathrm{m}$.

The sensitivity of polarization loss to the normal (transversal) tilt was obtained by finding the derivative of $\cos^2\alpha_\mathrm{TX}$ and $\cos^2\alpha_\mathrm{RX}$ from (18) with respect to α_TX and α_RX, respectively, for α_TX and α_RX equal to 5°, which is the center of the estimated interval of deviation [0°, 10°].

Table 1: Expanded uncertainties for various AUT heights.

	h = 0.5 λ	h = 1 λ	h = 1.25 λ	h = 1.5 λ	h = 2 λ
Combined standard uncertainty +/- U_c	2,341 dB	1,888 dB	2,860 dB	1,425 dB	2,920 dB
Expanded uncertainty +/- $2U_c$	**4,683 dB**	**3,776 dB**	**5,721 dB**	**2,850 dB**	**5,840 dB**

The sensitivity of G_{RX} to the longitudinal tilt of the respective antenna was obtained by finding its derivative with respect to ϑ. Functional dependence $G_{\mathrm{RX}} = f(\vartheta)$ is given by the expression for the gain of half-wave dipole (31). The estimated interval of deviation of the longitudinal tilt with respect to the elevation angle ϑ was [0°, 10°] around the elevation angle of $\vartheta = 45°$ (worst case, as explained in section 5.2). The obtained uncertainty (i.e. the same interval of deviation) was used also for the calculation of TX gain change ΔG_{TX} uncertainty, as explained in (20) and in Fig. 13.

Finally, the sensitivity of $|F|^2$ to the measured quantities h, d_{H}, d_{V}, and to the gain difference ΔG_{TX} from (20), was calculated. First, equation (20) was expressed using (3) – (9), (27), (28) and (29), obtaining the functional relationship $|F|^2 = f\left(h, d_{\mathrm{H}}, d_{\mathrm{V}}, \Delta G_{\mathrm{TX}}\right)$, and then the respective partial derivatives were calculated for each argument, according to (30). Due to complexity of the resulting equation, numerical values of the derivatives were computed by a mathematical software package. The worst-case scenario values $d_{\mathrm{H}} = d_{\mathrm{V}} = 3.95\,\mathrm{m}$ were used, together with ΔG_{TX} for the estimated interval of the longitudinal tilt deviation of [0°, 10°] around the elevation angle of $\vartheta = 45°$. However, the computations showed that the sensitivity coefficients of $|F|^2$ heavily depend on the AUT height h. Thus, the sensitivity coefficients of $|F|^2$ were computed separately for each AUT height h (0.5λ, 1λ, 1.25λ, 1.5λ and 2λ). Accordingly, the resulting combined uncertainty was also calculated separately for each AUT height h.

5.4 Uncertainty budget

The overall expanded uncertainty is shown in Table 1, separately for each AUT height h (0.5λ, 1λ, 1.25λ, 1.5λ and 2λ). The expanded uncertainty varies with AUT height, ranging from ±2.85 dB to ±5.84 dB (coverage factor $k = 2$). The detailed uncertainty budget is presented in Table 2.

The deviation intervals for all quantities were generally taken as worst cases. It is also important to note that these apply to the realized measurement setup prototype. Subsequent setups could surely be realized with more precision, especially concerning the most critical quantities. The largest contribution to the combined uncertainty comes from the array factor, and the single largest contribution comes from the uncertainty of the AUT height measurement above the sea surface. For our prototype, we estimated the AUT height measurement deviation of ±5 mm with rectangular distribution. A simulation shows that the overall expanded uncertainty could be narrowed to ±1.5 dB to ±2 dB if only the AUT height could be measured within ±1 mm, which is achievable with more precise setup. Other improvements could lower the uncertainty down to about ±1 dB (coverage factor $k = 2$).

6 CONCLUSION

A compact and innovative setup for measuring the elevation radiation pattern of an antenna above the sea surface has been proposed, realized and tested using half-wave dipole as the antenna under test (AUT).

The choice of frequency is connected with setup size limits. The presented setup greatest dimension was 4 m, appropriate for the chosen frequency of 2.48 GHz and AUT heights up to 2λ above the sea surface.

The proposed setup exhibits several innovative features, such as stable TX and RX antenna platforms (while the propagation path is still over sea surface) and straight movement of the receiving antenna during measurements (contrary to the usual concept of measurements along the arc). Due to the latter feature, the measurements were limited to the elevation angle range starting from the horizon up to a certain practical angle, 45° in this case. However, this range is fully adequate for most applications relating to terrestrial communications towards the horizon. The comparison of the measured patterns to the analytically calculated ones shows good agreement, with certain deviations that mainly fall within the boundaries of the calculated measurement uncertainty, which ranged from ±2.85 dB to ±5.84 dB (depending on the AUT height above the sea surface). The detailed analysis of uncertainty budget showed that further improvements are possible in terms of setup precision, that could lower the uncertainty down to the range from ±1 dB to ±2 dB.

As the proposed method and setup proved their usefulness with a well-known vertical half-wave dipole, the same method and setup (with possible improvements) could and will be used for testing other types of antennas.

REFERENCES

[1] C. A. Balanis, *Antenna theory, analysis and design*, New Jersey, USA: John Wiley & Sons, Inc., 2005.

Table 2: Uncertainty budget.

Contributions to uncertainty		Value	Units	Distribution	Divisor	Standard uncertainty	Sensitivity coefficient	Uncertainty
Power measurement, P	TX power measurement (constant power)	0,05	dB	rectangular	1,732	0,029	1	0,029 dB
	Linearity of spectrum analyzer log scale	1	dB	rectangular	1,732	0,577	1	0,577 dB
							Combined standard uncertainty $u_c(P)$	0,578 dB
Cable loss stability, L_c	Flexing (estimated)	0,2	dB	rectangular	1,732	0,115	1	0,115 dB
	Temperature stability (estimated)	0,15	dB	rectangular	1,732	0,087	1	0,087 dB
							Combined standard uncertainty $u_c(L_c)$	0,144 dB
TX antenna (AUT) height over sea, h	Scale resolution	0,0005	m	rectangular	1,732	0,000	1	0,000 m
	TX antenna positioning (ver. variation)	0,005	m	rectangular	1,732	0,003	1	0,003 m
							Combined standard uncertainty $u_c(h)$	0,003 m
Horizontal distance between TX and RX antenna, d_H	Scale resolution	0,0005	m	rectangular	1,732	0,000	1	0,000 m
	Scale deflection	0,01	m	rectangular	1,732	0,006	1	0,006 m
	RX antenna positioning (hor. variation)	0,1	m	rectangular	1,732	0,058	1	0,058 m
							Combined standard uncertainty $u_c(d_H)$	0,058 m
RX antenna height, d_V	Scale resolution	0,0005	m	rectangular	1,732	0,000	1	0,000 m
	RX antenna positioning (ver. variation)	0,0025	m	rectangular	1,732	0,001	1	0,001 m
							Combined standard uncertainty $u_c(d_V)$	0,001 m
Distance from TX phase center to RX antenna, squared, d^2	d_H	previously calculated $u_c(d_H)$				0,058	7,900	0,458 m^2
	d_V	previously calculated $u_c(d_V)$				0,001	7,900	0,012 m^2
							Combined standard uncertainty $u_c(d^2)$	0,459 m^2
								0,130 dB
Polarization effects on gain and losses, ΔG, ΔL	TX antenna normal tilt -> polarization loss	5	º	rectangular	1,732	0,050	0,174	0,009
	RX antenna parallel tilt -> gain change	5	º	rectangular	1,732	0,050	0,780	0,039
	RX antenna normal tilt -> polarization loss	5	º	rectangular	1,732	0,050	0,174	0,009
							Combined standard uncertainty	0,041
							$u_c(\Delta G, \Delta L)$	0,183 dB
Change in TX gain as a function of ϑ determined by measured distances, ΔG	h	previously calculated $u_c(h)$				0,003	0,121	0,000
	d_H	previously calculated $u_c(d_H)$				0,058	0,123	0,007
	d_V	previously calculated $u_c(d_V)$				0,001	0,121	0,000
							Combined standard uncertainty	0,007
							$u_c(\Delta G)$	0,031 dB
Change in RX gain as a function of ϑ determined by measured distances, ΔG	h	previously calculated $u_c(h)$				0,003	0,121	0,000
	d_H	previously calculated $u_c(d_H)$				0,058	0,123	0,007
	d_V	previously calculated $u_c(d_V)$				0,001	0,121	0,000
							Combined standard uncertainty	0,007
							$u_c(\Delta G)$	0,031 dB
Antenna array factor, squared (h = 0.5 λ), $\|F\|^2$	h	previously calculated $u_c(h)$				0,003	137,317	0,398
	d_H	previously calculated $u_c(d_H)$				0,058	0,757	0,044
	d_V	previously calculated $u_c(d_V)$				0,001	0,758	0,001
	ΔG_{TX}	= RX gain change due to parallel tilt				0,039	1,428	0,056
							Combined standard uncertainty	0,405
							$u_c(\|F\|^2)$	2,253 dB
Antenna array factor, squared (h = 1 λ), $\|F\|^2$	h	previously calculated $u_c(h)$				0,003	112,800	0,327
	d_H	previously calculated $u_c(d_H)$				0,058	0,853	0,049
	d_V	previously calculated $u_c(d_V)$				0,001	0,851	0,001
	ΔG_{TX}	= RX gain change due to parallel tilt				0,039	1,434	0,056
							Combined standard uncertainty	0,336
							$u_c(\|F\|^2)$	1,777 dB
Antenna array factor, squared (h = 1.25 λ), $\|F\|^2$	h	previously calculated $u_c(h)$				0,003	156,977	0,455
	d_H	previously calculated $u_c(d_H)$				0,058	2,029	0,118
	d_V	previously calculated $u_c(d_V)$				0,001	2,032	0,003
	ΔG_{TX}	= RX gain change due to parallel tilt				0,039	1,437	0,056
							Combined standard uncertainty	0,474
							$u_c(\|F\|^2)$	2,788 dB
Antenna array factor, squared (h = 1.5 λ), $\|F\|^2$	h	previously calculated $u_c(h)$				0,003	77,073	0,224
	d_H	previously calculated $u_c(d_H)$				0,058	1,845	0,107
	d_V	previously calculated $u_c(d_V)$				0,001	1,847	0,003
	ΔG_{TX}	= RX gain change due to parallel tilt				0,039	1,440	0,057
							Combined standard uncertainty	0,254
							$u_c(\|F\|^2)$	1,274 dB
Antenna array factor, squared (h = 2 λ), $\|F\|^2$	h	previously calculated $u_c(h)$				0,003	154,427	0,448
	d_H	previously calculated $u_c(d_H)$				0,058	2,859	0,166
	d_V	previously calculated $u_c(d_V)$				0,001	2,865	0,004
	ΔG_{TX}	= RX gain change due to parallel tilt				0,039	1,446	0,057
							Combined standard uncertainty	0,481
							$u_c(\|F\|^2)$	2,850 dB

[2] A. De, T. K. Sarkar, M. Salazar-Palma, "Characterization of the far-field environment of the antennas located over a ground plane and implications for cellular communication systems," in *IEEE Antennas and Propagation Magazine*, vol. 52, no. 6, pp. 19-40, December 2010.

[3] D. Senić, A. Šarolić, "Simulation of a shipboard VHF antenna radiation pattern using a complete sailboat model," in *17th International Conference on Software, Telecommunications & Computer Networks SoftCOM 2009*, (Hvar, Croatia), pp. 1-5, September 2009.

[4] D. Senić, A. Šarolić, "Simulation of slanted shipboard VHF antenna radiation pattern," in *Proceedings of 52nd International Symposium ELMAR-2010*, (Zadar, Croatia), pp. 293-296, September 2010.

[5] R. E. Collin, "Hertzian dipole radiating over a lossy earth or sea: some early and late 20th-century controversies," in *IEEE Antennas and Propagation Magazine*, vol. 46, no. 2, pp. 64-79, April 2004.

[6] R. W. P. King, S. S. Sandler, "The electromagnetic field of a vertical electric dipole over the Earth or sea," in *IEEE Transactions on Antennas and Propagation*, vol. 42, pp. 382-389, March 1994.

[7] L. Liu, K. Li, "Radiation from a vertical electric dipole in the presence of a three-layered region," in *IEEE Transactions on Antennas and Propagation*, vol. 55, pp. 3469-3475, December 2007.

[8] A. Šarolić, B. Modlic, D. Poljak, "Measurement validation of ship wiregrid models of different complexity," in *2001 IEEE International Symposium on Electromagnetic Compatibility*, (Montreal, Canada), pp. 147-150., August 2001.

[9] F. Schlagenhaufer, "Computer simulation of shipboard communications antennas," in *IEEE 6th International Symposium on Electromagnetic Compatibility and Electromagnetic Ecology*, pp. 315–318, June 2005.

[10] A. Šarolić, B. Modlic, K. Malarić, "Shipboard HF electromagnetic field measurements for EMC," in *Proceedings TEMI 2001, 11th IMEKO TC-4 Symposium on Trends in Electrical Measurement and Instrumentation*, (Lisbon, Portugal), pp. 38-42, September 2001.

[11] D. J. Travers, B. B. Peterson, M. E. McKaughan, D. E. Fessenden, "Measured and predicted field patterns of MF/HF communication antennas on US Coast Guard patrol boats," in *1990 IEEE Antennas and Propagation Society International Symposium*, (Dallas, USA), pp. 1859-1862, May 1990.

[12] D. E. Fessenden, D. C. Portofee, "Predicted performance of the NUSC 70 foot over sea water antenna pattern arch," in *1982 IEEE Antennas and Propagation Society International Symposium*, vol. 20, pp. 386-389, May 1982.

[13] J.A. Stratton, H.A. Chinn, "The radiation characteristics of a vertical half-wave antenna," in *Proceedings of the Institute of Radio Engineers*,vol. 20, no. 12, pp. 1892-1913, 1932.

[14] A. Šarolić, D. Senić, Z. Živković, "Some preliminary results of radiation pattern measurements for a vertical dipole over sea" in *Proceedings of 53rd International Symposium ELMAR-2011*, (Zadar, Croatia), pp. 341-344, September 2011.

[15] C. A. Balanis, *Advanced engineering electromagnetics*, USA: John Wiley & Sons, Inc., 1989.

[16] Rec. ITU-R P.527-3, "Electrical Characteristics of the Surface of the Earth," 1992.

[17] 4NEC2 antenna modeler and optimizer, version 5.7.5, http://home.ict.nl/ ˜arivoo

[18] H. R. Chuang, L. C. Kuo, "3-D FDTD design analysis of a 2.4-GHz polarization-diversity printed dipole antenna with integrated balun and polarization-switching circuit for WLAN and wireless communication applications," in *IEEE Transactions Microwave Theory and Techniques*, vol. 51, no. 2, pp. 374-381, February 2003.

[19] "The expression of uncertainty in EMC testing," UKAS Publication LAB 34, Edition 1, 2002.

[20] JCGM 100:2008. "Evaluation of measurement data – Guide to the expression of uncertainty in measurement" (GUM 1995 with minor corrections)

Antonio Šarolić received the Diploma Engineer, MS and PhD degrees in Electrical Engineering in 1995, 2000 and 2004 from the University of Zagreb, Croatia. He was employed at the same university from 1995 to 2005, at the Faculty of Electrical Engineering and Computing (FER), Dept. of Radiocommunications. In 2006 he joined the University of Split, Faculty of Electrical Engineering, Mechanical Engineering and Naval Architecture, and is now Associate Professor in Electrical Engineering and Head of Chair of Applied Electromagnetics. His areas of interest are electromagnetic mea-

surements, radiocommunications, electromagnetic compatibility (EMC) and biological effects of electromagnetic fields. Since 2008 he has been the leader of the research project "Measurements in EMC and EM health effects research". He is the chairman of the Croatian standardization technical committees E106 "Electromagnetic fields in human environment" and E80 "Maritime navigation and radiocommunication equipment and systems", chairman of the IEEE EMC Society - Croatia Chapter, and member of the Management Committee of the COST Action BM0704 "Emerging EMF Technologies and Health Risk Management". He is a member of IEEE, IEICE and BEMS.

Damir Senić received the Diploma Engineer degree in Electrical Engineering in 2008 from the Faculty of Electrical Engineering, Mechanical Engineering and Naval Architecture, University of Split, Croatia. He is currently a research assistant and PhD student at the University of Split, Faculty of Electrical Engineering, Mechanical Engineering and Naval Architecture (FESB), Department of Electronics. His research interests are: electromagnetic measurements, bioeffects of EM fields, electromagnetic compatibility (EMC) and radiocommunications.

Zlatko Živković received the Diploma Engineer degree in Electrical Engineering in 2007 from the Faculty of Electrical Engineering, Mechanical Engineering and Naval Architecture, University of Split, Croatia. He is currently a research assistant and PhD student at the University of Split, Faculty of Electrical Engineering, Mechanical Engineering and Naval Architecture (FESB), Department of Electronics. His research interests are: electromagnetic measurements, bioeffects of EM fields, electromagnetic compatibility (EMC) and radiocommunications.

AUTHORS' ADDRESSES

Prof. Antonio Šarolić, Ph.D.
Damir Senić
Zlatko Živković
Faculty of Electrical Engineering, Mechanical Engineering and Naval Architecture (FESB)
University of Split
Ruđera Boškovića 32, HR-21000 Split, Croatia
email: antonio.sarolic@fesb.hr, damir.senic@fesb.hr, zlatko.zivkovic@fesb.hr

Received: 2012-01-10
Accepted: 2012-01-23